

TIDAL SENSITIVITY OF LOW-FREQUENCY EARTHQUAKES ON THE  
SAN ANDREAS FAULT - ANALYSIS OF A DECLUSTERED CATALOG

by

ALEXANDER MICHAEL BABB

A THESIS

Presented to the Department of Earth Sciences  
and the Graduate School of the University of Oregon  
in partial fulfillment of the requirements  
for the degree of  
Master of Science

December 2018

THESIS APPROVAL PAGE

Student: Alexander Michael Babb

Title: Tidal Sensitivity of Low-Frequency Earthquakes on the San Andreas Fault -  
Analysis of a Declustered Catalog

This thesis has been accepted and approved in partial fulfillment of the requirements for  
the Master of Science degree in the Department of Earth Sciences by:

Amanda Thomas	Chairperson
Alan Rempel	Member
Diego Melgar	Member

and

Janet Woodruff-Borden	Vice Provost and Dean of the Graduate School
-----------------------	--

Original approval signatures are on file with the University of Oregon Graduate School.

Degree awarded December 2018

© 2018 Alexander Michael Babb

## THESIS ABSTRACT

Alexander Michael Babb

Master of Science

Department of Earth Sciences

December 2018

Title: Tidal Sensitivity of Low-Frequency Earthquakes on the San Andreas Fault -  
Analysis of a Declustered Catalog

Low frequency earthquakes (LFEs) are detected at depths of 16-30 km on a 150 km section of the San Andreas Fault (SAF) centered at Parkfield, CA. The LFEs are divided into 88 families based on waveform similarity. In continuous families a burst of a few LFE events recurs every few days while episodic families experience essentially quiescent periods often lasting months followed by bursts of hundreds of events over a few days. The occurrence of LFEs has also been shown to be sensitive to extremely small ( $\sim 1$  kPa) tidal stress perturbations. However, the clustered nature of LFE occurrence could potentially bias estimates of tidal sensitivity. Here we re-evaluate the tidal sensitivity of LFE families on the deep San Andreas using a declustered catalog. Declustered LFE families are still highly sensitive to primarily right-lateral shear stress (RLSS) and to a lesser extent fault normal stress (FNS).

## CURRICULUM VITAE

NAME OF AUTHOR: Alexander Michael Babb

### GRADUATE AND UNDERGRADUATE SCHOOLS ATTENDED:

University of Oregon, Eugene  
University of Nebraska at Omaha

### DEGREES AWARDED:

Master of Science, Earth Sciences, 2018, University of Oregon  
Bachelor of Science, Geological Sciences, 2016, University of Nebraska at  
Omaha

### AREAS OF SPECIAL INTEREST:

Seismology

### PROFESSIONAL EXPERIENCE:

General Employee, University of Oregon, 2016-2018

### PUBLICATIONS:

Babb, A.M., Thomas, A.M., Bletery, Q. (2017) Tidal Sensitivity of Declustered Low Frequency Earthquake Families and Inferred Creep Episodes on the San Andreas Fault. AGU Fall Meeting

## ACKNOWLEDGMENTS

First, I wish to express my sincerest gratitude to my advisor Amanda Thomas for her support and guidance throughout this research project, without which this would not have been possible. In addition, I thank my committee members Alan Rempel and Diego Melgar for their helpful thesis edits. I also thank Matt Polizzotto for his keen eye and way with words. A special thanks to Marla Trox, Sandy Thoms, and Dave Stemple for helping facilitate the process of completing my graduate degree. To Ava and Atlas, I am grateful for their neutral stance on my scientific work and pawsitive perspectives on all matters pet related. Lastly, to my parents and siblings, without whom I would not have come so far, thank you all for you love and support through everything.

## TABLE OF CONTENTS

Chapter	Page
I. INTRODUCTION.....	1
II. METHODS.....	10
LFE Catalog.....	10
Declustering the LFE Catalog.....	10
Schuster Test and Spectra.....	11
Percent Excess.....	17
III. RESULTS.....	20
Schuster Spectra.....	20
Spatial Distribution of LFE Family Sensitivity to Tidal Stresses.....	20
RLSS $N_{ex}$ vs Declustered RLSS $N_{ex}$ .....	26
IV. DISCUSSION.....	28
$N_{ex}$ Values.....	28
Schuster Spectra.....	30
V. CONCLUSIONS.....	32
REFERENCES CITED.....	34

## LIST OF FIGURES

Figure	Page
1. Parkfield, CA area location map with LFE locations plotted as circles and squares, representing continuous and episodic LFE families, respectively.....	5
2. Example time series in 2007 of cumulative number of LFEs over a four-month time period for three LFE families (55, 19, and 85).....	8
3. LFE distribution of continuous family 5.....	12
4. LFE distribution of episodic family 55.....	13
5. Schuster walk of clustered LFE family 9 tested at the tidal period of N2 (12.658 hr).....	15
6. Schuster walk of declustered LFE family 9 tested at the tidal period of N2 (12.658 hr).....	16
7. Time series of tidally induced shear (red) and normal (blue) stresses computed over a period of approximately two weeks for the SAF .....	18
8. Schuster spectrum of original LFE family 9 catalog .....	21
9. Schuster spectrum of declustered LFE family 9 catalog .....	22
10. Schuster spectra results for all continuous and episodic LFE families.....	23
11. Cross section of SAF centered beneath Parkfield (0 km) with LFE locations color-coded by $N_{ex}$ values and plotted as circles and squares, representing continuous and episodic families, respectively.....	24
12. Original LFE catalog $N_{ex}$ values plotted against declustered LFE catalog $N_{ex}$ values plotted as circles and squares, representing continuous and episodic families, respectively .....	27



LIST OF TABLES

Table	Page
1. Tidal constituents present at Parkfield, CA .....	9

# CHAPTER I

## INTRODUCTION

The lithospheric plates that compose the surface of the earth move at rates of up to 10s of mm/yr (Ryder and Burgmann, 2008; Murray et al. 2001; Thatcher and Lisowski, 1987). At their boundaries, the plates accommodate this motion on faults, or localized zones of deformation that accommodate slip through multiple mechanisms. For example, some faults gradually build up elastic strain over a time period and then abruptly release it during an earthquake, which can generate strong ground motion felt by humans. Alternatively, faults can slide stably, slipping at rates that are not sufficient to generate seismic waves. The majority of fault zones world-wide host large earthquakes in their shallow seismogenic regions and deform aseismically below the brittle-ductile transition, where pressure and temperature conditions are amenable to plastic deformation (Scholz, 2002). Traditionally, a section of fault is classified as either “seismic”, meaning it is capable of hosting an earthquake, or “aseismic” meaning slip is never accommodated at seismic slip speeds. The discoveries of slow-slip phenomena, such as non-volcanic tremor (NVT) (Obara, 2002), periodic slow slip events (SSEs) (Rodgers and Dragert, 2003), and low-frequency earthquakes (LFEs) below the seismogenic zone (Shelly et al., 2007a) reveal that the characterization of fault slip as seismic or aseismic is too restrictive. Instead, any given section of fault can accommodate deformation through multiple mechanisms that occur over different timescales (Ide et al., 2007a; Beroza and Ide, 2011).

A slow slip event (SSE) is the aseismic slip of a fault patch that occurs below velocities required to generate appreciable seismic radiation, resulting in event durations

of hours to days (Schwartz and Rokosky, 2007). These silent events went undetected until the broad implementation of high resolution Global Position System (GPS) networks, which have allowed for the detection of SSEs in Japan (Hirose et al., 1999; Ozawa et al., 2001), Cascadia (Dragert et al., 2001), Mexico (Lowry et al., 2001), Alaska (Freymueller et al., 2002), and elsewhere. A SSE's geodetic signal manifests as a transient reversal of longer-term plate motion (Hirose et al., 1999; Dragert et al., 2001). GPS inversion of displacements during recurrent SSEs in the Cascadia subduction zone results in strain releases equivalent to  $M_w \sim 6$  earthquakes over durations of several weeks (Schmidt et al., 2010).

Shortly after the discovery of SSEs, a seismic signal dubbed NVT, was found to correlate temporally and spatially with SSEs on the subducting Philippine Sea plate in southwest Japan (Obara et al., 2004; Hirose and Obara, 2005) and the Cascadia subduction zone (Rogers and Dragert, 2003). NVT was also detected on the deep San Andreas Fault (Nadeau and Dolenc, 2005; Nadeau and Guilhem, 2009). NVT is different from ordinary recorded earthquakes in that it lacks impulsive P- and S-wave arrivals, has dominant amplitudes at lower frequencies of 1-10 Hz with rapid amplitude decay at increasing frequencies, and durations on the order of minutes to days (Kao et al. 2005; Shelly et al., 2007b). The coupled phenomenon of tremors occurring simultaneously with SSEs is termed episodic tremor and slip (ETS) (Rogers and Dragert, 2003). In subduction zones and strike-slip faults, ETS occurs near the transition zone, where the updip plate transitions from being frictionally locked to stable sliding (Obara and Hirose, 2006; Shelly et al., 2006). During ETS, the aseismic slip front can propagate at rates of up to 15 km/day along the plate interface, and often includes tremor migration (Dragert and

Rogers, 2004; Obara, 2002; Obara et al., 2004; Schmidt et al., 2010). The NVT is thought to represent simultaneous seismic failure of numerous asperities embedded within an aseismically slipping matrix (Shelly et al., 2006; Ito et al., 2007).

The Japan Meteorological Agency (JMA) created a new class of events, called low-frequency earthquakes (LFEs), in 1999 after their detection using a newly installed dense network of highly sensitive short-period seismometers. Despite not knowing the nature of LFE occurrence, the JMA started cataloging the events (Nishide et al., 2000). LFEs were later found to temporally and spatially occur mostly as part of tremor episodes (Obara and Hirose, 2006), like the ETS in Cascadia. Shelly et al. (2007b), using high quality LFEs as template events, systematically searched tremor for matching waveforms revealing a nearly continuous sequence of LFEs during periods of active tremor. This established the idea that tremor results from the superposition of numerous LFEs and is believed to be generated by shear slip on the fault considering the consistent focal mechanisms between individual LFEs and SSEs (Ide et al. 2007b; Shelly et al., 2007b). While the spectral characteristics of tremor and LFEs are essentially identical, high-quality low-noise recordings of LFEs frequently contain S-wave arrivals, which allow for better constraint on hypocentral locations (Shelly et al., 2006). To further constrain locations, combinations of stacked waveform cross-correlation and double-difference tomography can be employed (Shelly et al., 2006).

NVT and LFEs have both been noted for their extreme sensitivity to small stress perturbations. Studies of stress changes on the SAF due to the 2003  $M_w$  6.5 San Simeon and the 2004  $M_w$  6.0 Parkfield earthquakes discovered increased tremor rates in areas with increased shear-stresses of 6 to 9 kPa respectively (Nadeau and Guilhem, 2009;

Shelly and Johnson, 2011). NVT triggering in response to teleseismic surface and body waves with stress transients on the order of kilopascals has been observed in multiple studies (Gomberg et al., 2008; Miyazawa and Brodsky, 2008; Peng et al., 2009; Rubinstien et al., 2007). Most notably, studies of tidal stress perturbations have confirmed that NVTs are sensitive to stress changes as small as fractions of a kilopascal in Japan, Cascadia, and the San Andreas Fault (Rubinstein et al., 2008; Nakata, et al. 2008; Lambert et al. 2009; Thomas et al. 2009, Thomas et al., 2012). Previous work by Thomas et al. (2012) established LFE sensitivity to tidally induced stress components on the SAF using a decade-long catalog of events. This thesis builds on their work to establish LFE sensitivity to tidally induced stresses on the deep San Andreas Fault (SAF).

The San Andreas Fault is a right-lateral strike-slip fault that extends approximately 1,200 km across California, separating the Pacific Plate from the North American Plate. In this study we focus on a 150 km transitional segment centered on Parkfield, CA (Fig. 1). The SAF to the northwest of Parkfield is characterized predominately by creep and hosts numerous small magnitude earthquakes. To the southeast the fault is thought to be locked and few earthquakes have been recorded (Burford and Harsh, 1980; Shulz et al., 1982; Argus and Gordon, 2001). The locked portion was last ruptured in the  $M_w$  7.8 1857 Fort Tejon earthquake, which is thought to have nucleated near Parkfield (Sieh, 1978). The section directly beneath Parkfield has hosted six  $M_w$  5.5 – 6.5 earthquakes since 1881, with the most recent being 2004.

Shelly and Hardebeck (2010) successfully cataloged 88 LFE families along the SAF, comprising over 550,000 individual LFEs grouped based on waveform similarity. Centered at Parkfield, CA the families range in depth from the base of the seismogenic

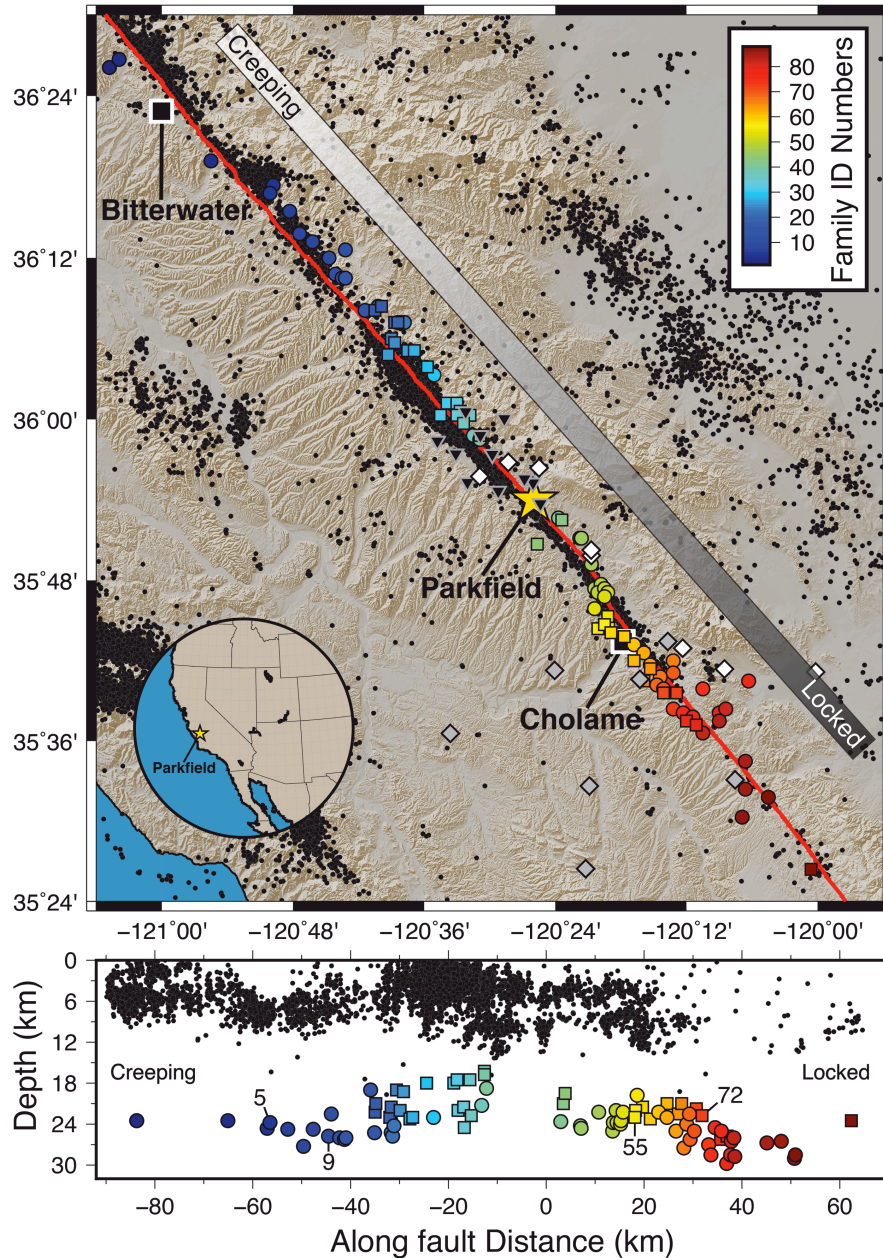


Fig. 1. (top) Parkfield, CA area location map with LFE locations plotted as circles and squares, representing continuous and episodic LFE families, respectively, color-coded by family ID numbers starting in the northwest and ending in the southeast along the fault. Relocated earthquakes (post 2001) from the catalog of Waldhauser and Schaff (2008) are shown as black dots. The San Andreas Fault is delineated in red. Surface seismic stations used for detection and borehole stations used for locations are shown by white and grey diamonds and black triangles respectively. The cities of Bitterwater and Cholame are labeled by black squares with white outlines and Parkfield a yellow star. (bottom) Along-fault cross section of the SAF, centered at Parkfield (0 km) and viewed from the southwest, showing locations of LFE families from the top panel color-coded by their family ID number. Reference families are labeled by their ID numbers. Relocated earthquakes within 10 km of the fault from the top panel are plotted as black dots.

zone to the top of the Moho (16-30 km) and span just over 80 km to the north and 60 km to the south on the SAF. The families are split into northern and southern groups by a 15 km quiescent gap directly beneath Parkfield, CA. Tremor activity within the families varies from highly episodic to nearly continuous (Fig. 2). Episodic families tend to reside more shallowly and can have concentrated periods of high activity, with more than 200 LFEs in less than a week, followed by multiple months of dormancy. Continuous families tend to reside at greater depth and often have a period of a few events recurring every 3-5 days.

The Earth is influenced by tidal forces which arise from the gravitational fields of the Sun and Moon. These forces produce deformations in the solid Earth and ocean. On large length scales the crust of the Earth is considered to be elastic, and as so experiences elastic deformation in response to the gravitational changes caused by the orbits of the Sun and Moon. The solid Earth deformations are called body tides. At low latitudes the surface of the Earth moves vertically through a range greater than 40 cm in just over 6 hours (Baker, 1984). For our research area, the magnitude of stresses in the crust induced by body tides are on the order of kPa and are far enough inland that ocean tidal loading does not significantly contribute to the stresses (Thomas et al., 2012). Two dominant tidal cycles, termed diurnal and semidiurnal, arise. Diurnal tides are characterized by a single high tide and low tide every day. Semidiurnal tidal cycles experience two high and two low tides of approximately equal magnitude each day. The combined signals of these two tidal cycles produce a mixed semidiurnal tidal cycle of two high and two low tides of different magnitudes each day. Because the Moon orbits in the same direction of the Earth's rotation, a lunar day is approximately 24 hours and 50 minutes whereas a solar

day is 24 hours. The tidal periods of interest for this project are listed in Table 1.



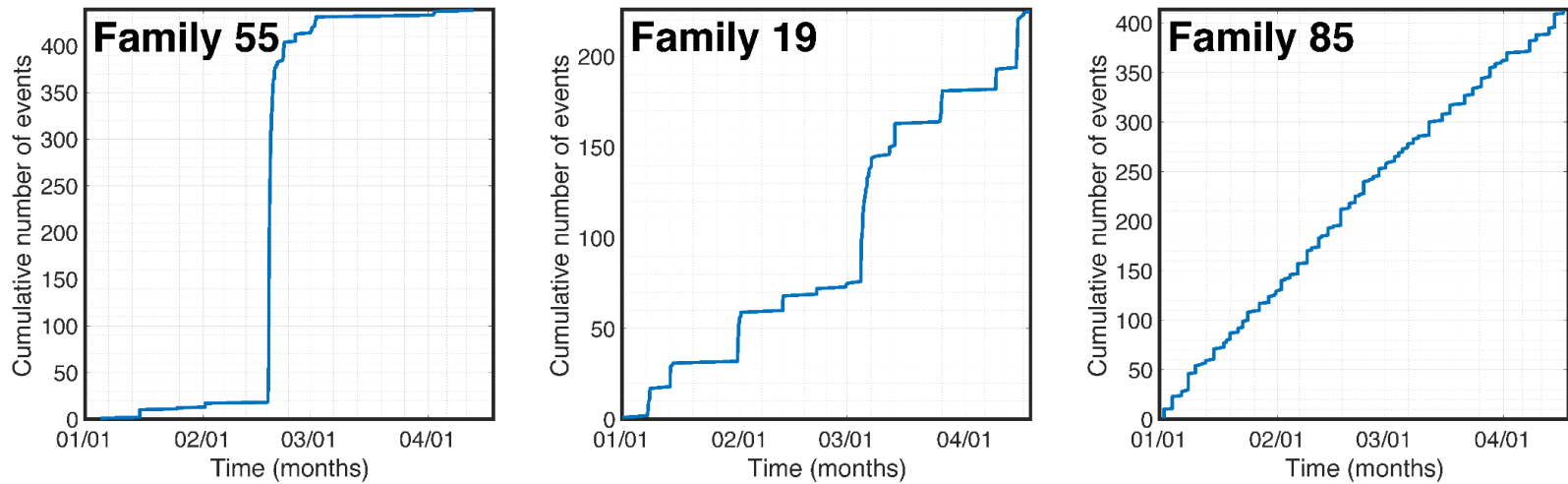


Figure 2. Example time series in 2007 of cumulative number of LFEs over a four-month time period for three LFE families (55, 19, and 85). Family 55 is highly episodic with quiescent periods of months punctuated by periods of days with extremely high LFE rates. Family 85 is a continuous family with small quiescent periods of less than a week, frequently interspersed with LFE episodes of smaller magnitude than family 55. Family 19 exemplifies the transitional behavior between the two endmembers of episodic and continuous LFEs.

**Table 1.** Tidal constituents present at Parkfield, CA

<b>Tidal constituents</b>	<b>Symbol</b>	<b>Period (h)</b>	<b>FFT amplitude (Pa)</b>	
Semidiurnal			FNS	RLSS
Lunisolar	K <sub>2</sub>	11.97	112.26	20.30
Principal solar	S <sub>2</sub>	12.00	399.63	80.63
Principal lunar	M <sub>2</sub>	12.42	695.09	91.49
Larger lunar elliptic	N <sub>2</sub>	12.66	149.15	18.37
Diurnal				
Lunar	K <sub>1</sub>	23.93	885.98	77.98
Solar*	S <sub>1</sub>	24.00	5.82	0.52
Solar	P <sub>1</sub>	24.07	286.91	25.52
Lunar	O <sub>1</sub>	25.82	589.53	54.94
Larger lunar elliptic	Q <sub>1</sub>	26.87	113.95	10.97

\*Diurnal solar constituent S<sub>1</sub> does not have an appreciable amplitude at Parkfield.

## CHAPTER II METHODS

### **LFE Catalog**

This study utilizes a declustered low-frequency earthquake catalog of over 80,000 LFE clusters from Thomas et. al. (2018). The original catalog was produced by Shelly and Hardebeck (2010), who grouped more than 500,000 LFEs into 88 unique families using waveform templates. To create a template, a single LFE event is visually identified from seismic records at a borehole station near the fault. The event is then cross-correlated every 0.05 s through the previous eight years of borehole data and the 100 most similar events are stacked into a master template. Waveform stacks are then created at all California Integrated Seismic Network stations by combining the 400 events in each family that have the highest summed correlation with the master template. This technique improves the signal to noise ratio, resolving clear P- and S-wave arrivals. The hypocentral locations are determined from both P- and S-wave arrivals and the 3D seismic velocity structure.

### **Declustering the LFE Catalog**

To decluster the original catalog, Thomas et al. employed a method using recurrence intervals between individual LFEs within given families (2018). For each LFE family the time between an LFE and its previous event was calculated, creating a list of interevent times or recurrence intervals,  $T_r$ . A smoothed histogram of  $\log(T_r)$  is plotted as a function of time using step sizes of 0.1 and bin widths of 0.6 log (days). For all LFE families the recurrence intervals separated into two or three distinct populations with local maxima separated by local minima. The values of the local minima were used to separate the individual LFEs of a given family into their respective populations. For

continuous families, the interevent times separated into two distinct groups of short and long populations (Fig. 3). Episodic families have three groups representing short, intermediate, and long populations (Fig. 4). In both continuous and episodic families, the long recurrence interval populations are thought to represent the first LFE event in a creep episode with the short recurrence interval populations being LFEs contained within an ongoing episode. Episodic families also include a third intermediate population, which is characteristic of the first LFE event within short-duration episodes, or “bursts” occurring within the longer duration episode.

### **Schuster Test and Spectra**

To confirm that the catalog from Thomas et al. (2018) was successfully declustered, the catalog was evaluated using the Schuster spectrum. The Schuster spectrum is an extension of the Schuster test and was developed by Ader and Avouac (2013) with the purpose of detecting periodicities in seismicity rates. The Schuster spectrum can also be used to determine whether or not a catalog has been properly declustered, and it works by performing a set of numerous individual Schuster tests over a continuous range of periods. The Schuster test provides the statistical probability that the distribution of the event times relative to a periodic perturbation results from a uniform random process. This value allows for the rejection of the null hypothesis that events from a catalog do not correlate with a specified period. In the LFE catalog, each event represents a phasor with a unit length and an angle corresponding to the event time on a  $360^\circ$  trigonometric circle. For example, testing for a period of 24 hours, event times of 12 AM, 6 AM, 12 PM, and 6 PM would have angles of  $0^\circ$ ,  $90^\circ$ ,  $180^\circ$ , and  $270^\circ$  respectively. P-values can

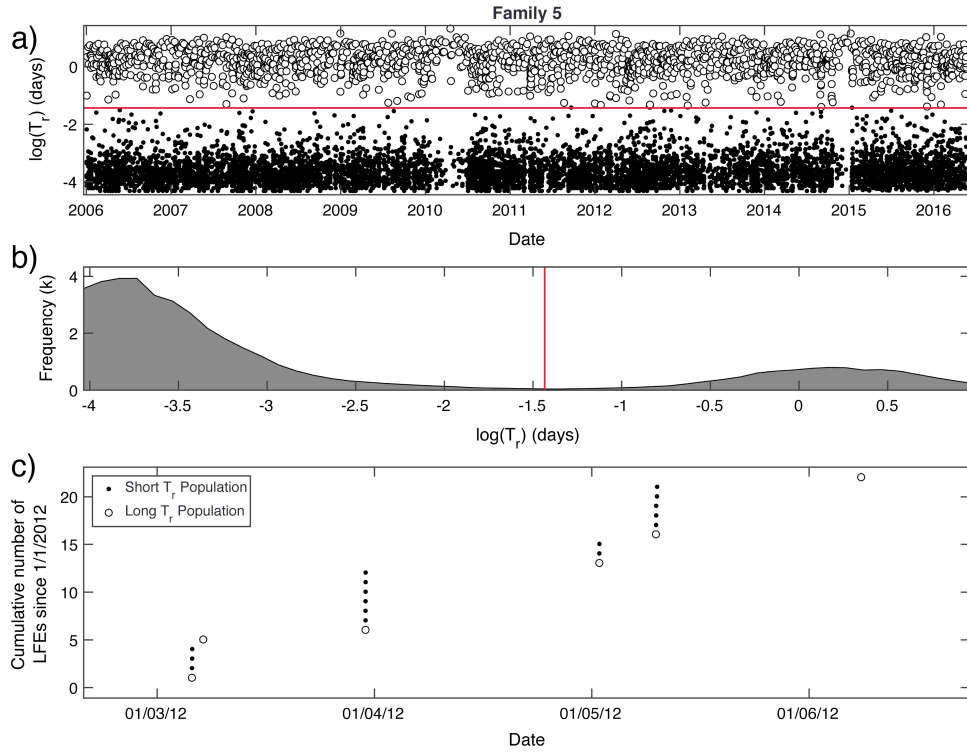


Figure 3. LFE distribution of continuous family 5. (a) Date versus  $\log(T_r)$  for continuous family 5. Red horizontal lines mark boundaries between recurrence interval populations. (b) Smoothed histogram of  $\log(T_r)$ . Local minima are marked by vertical red lines. The values are used to separate each individual LFE in family 5 into populations of events with similar preceding recurrence intervals. (c) Cumulative number of events versus time plot for family 5 for 4 days in 2012. Each individual LFE occurrence is indicated by the symbol corresponding to the long and short  $\log(T_r)$  populations. Legend in Figure 3c shows the definition of duration for a given episode. Figure from Thomas et al. (2018).

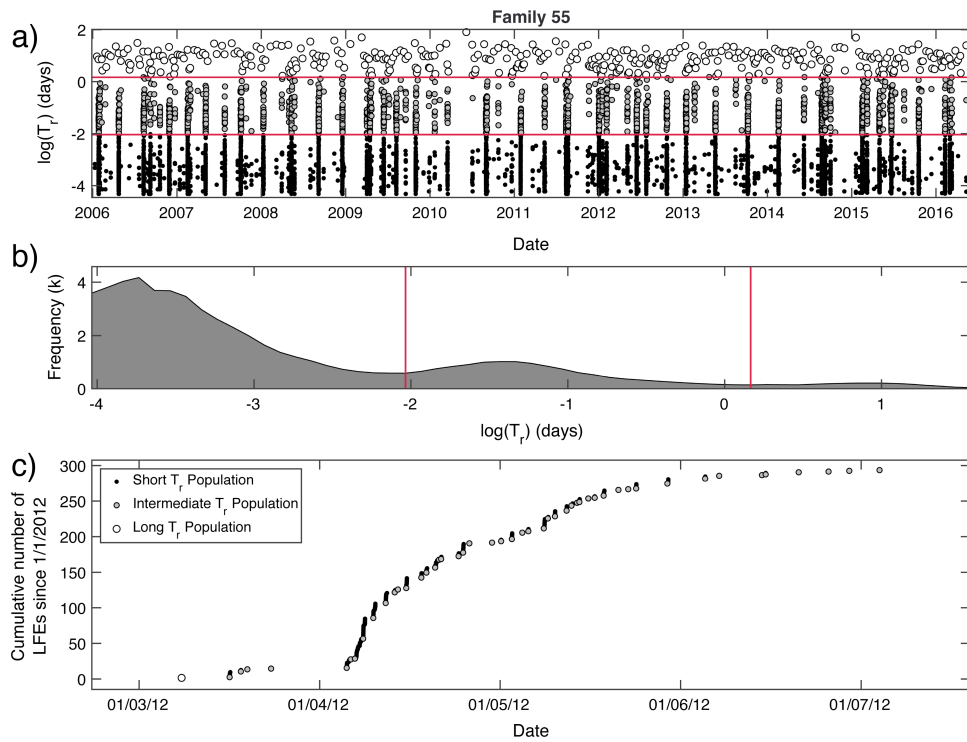


Figure 4. LFE distribution of episodic family 55. (a) Date versus  $\log(T_r)$  for episodic family 55. Red horizontal lines mark boundaries between recurrence interval populations. (b) Smoothed histogram of  $\log(T_r)$ . Local minima are marked by vertical red lines. The values are used to separate each individual LFE in family 55 into populations of events with similar recurrence intervals. (c) Cumulative number of events versus time plot for family 55 for 5 days in 2012. Each individual LFE occurrence is indicated by the symbol corresponding to the long, intermediate, and short  $\log(T_r)$  populations. Legend in Figure 4c shows the definition of duration for a given episode. Figure from Thomas et al. (2018).

be calculated with respect to sine-wave functions of specified period  $T$ . Each event is assigned a phase  $\theta_k$ , where  $t_k$  is the time of event number  $k$ :

$$\theta_k = 2\pi \frac{t_k}{T}$$

The phasors are plotted as unit length steps in the direction of their corresponding phase angle. The distance between the origin and the endpoint of the walk is  $D$ , with  $N$  being the number of events in the considered catalog. The probability  $p$ , that a distance of  $D$  can be reached by a uniformly random two-dimensional walk, is equivalent to the probability of the null hypothesis that the event times are distributed from a uniform seismicity rate (Schuster, 1897; Ader and Avouac, 2013)

$$p = e^{-D^2/N}$$

This equation calculates what is referred to as the Schuster p-value. A lower p-value indicates higher probability that the events stacked over period  $T$  are non-uniform, giving the probability of periodicity at the specified period  $T$ . Figure 5 shows an example of a single Schuster test for LFE family 9, testing the tidal period of N2 (12.658 hr), resulting in a p-value low enough to reject the null hypothesis of a uniform seismicity rate signifying a significant non-uniform component to seismicity at the period tested. The previous test was repeated on the declustered catalog of the same family, shown in Figure 6, and failed to reject the null-hypothesis.

## Schuster Walk - LFE Family 9

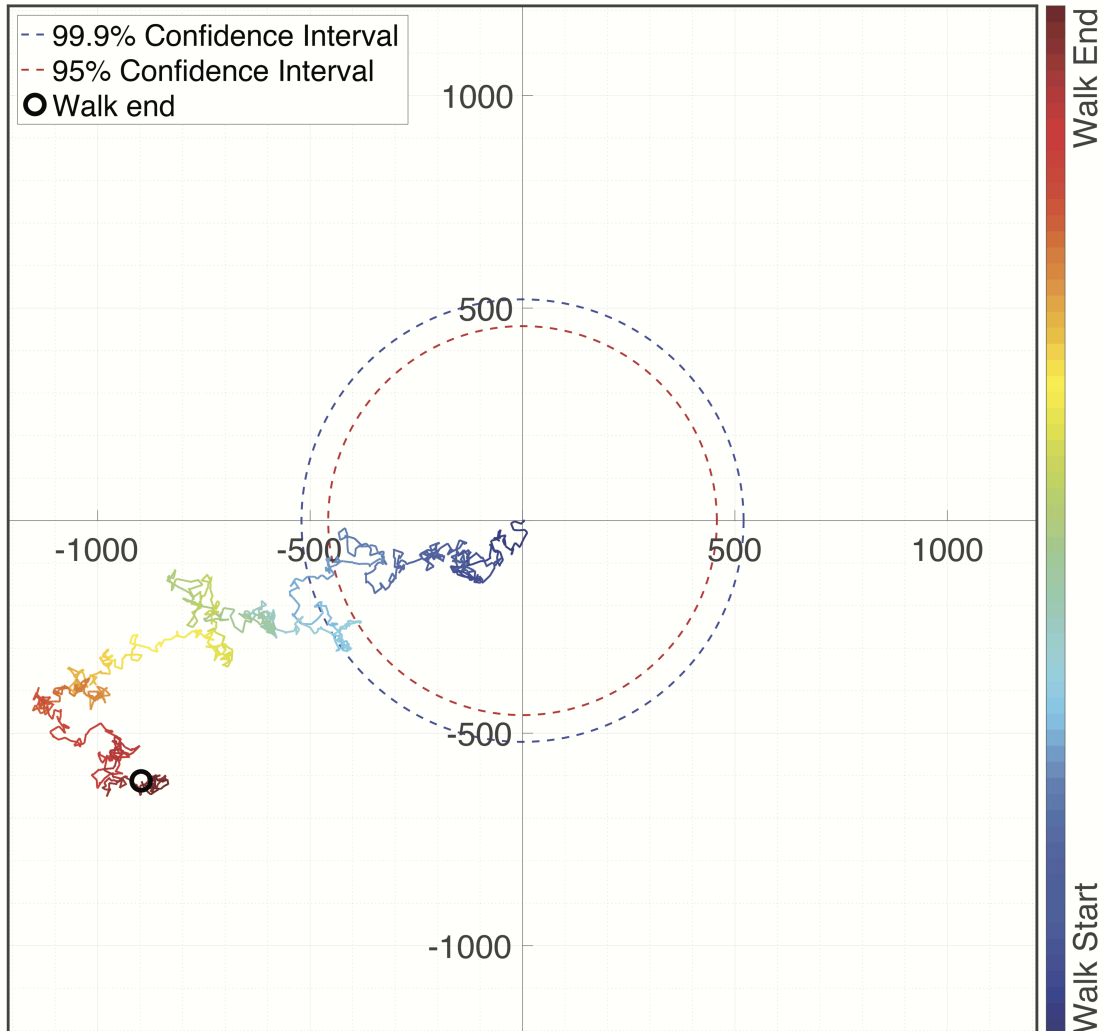


Figure 5. Schuster walk of LFE family 9 tested at the tidal period of N2 (12.658 hr) with a result indicating a non-uniform component to seismicity. Walk initiates at the origin in dark blue and finishes inside the black circle in dark red. The blue and red dashed lines represent the 99.9% and 95% confidence intervals respectively. The black outlined circle locates the walk's end. The test returns a significant result when the walk ends outside of the respective confidence interval.



## Schuster Walk - LFE Family 9

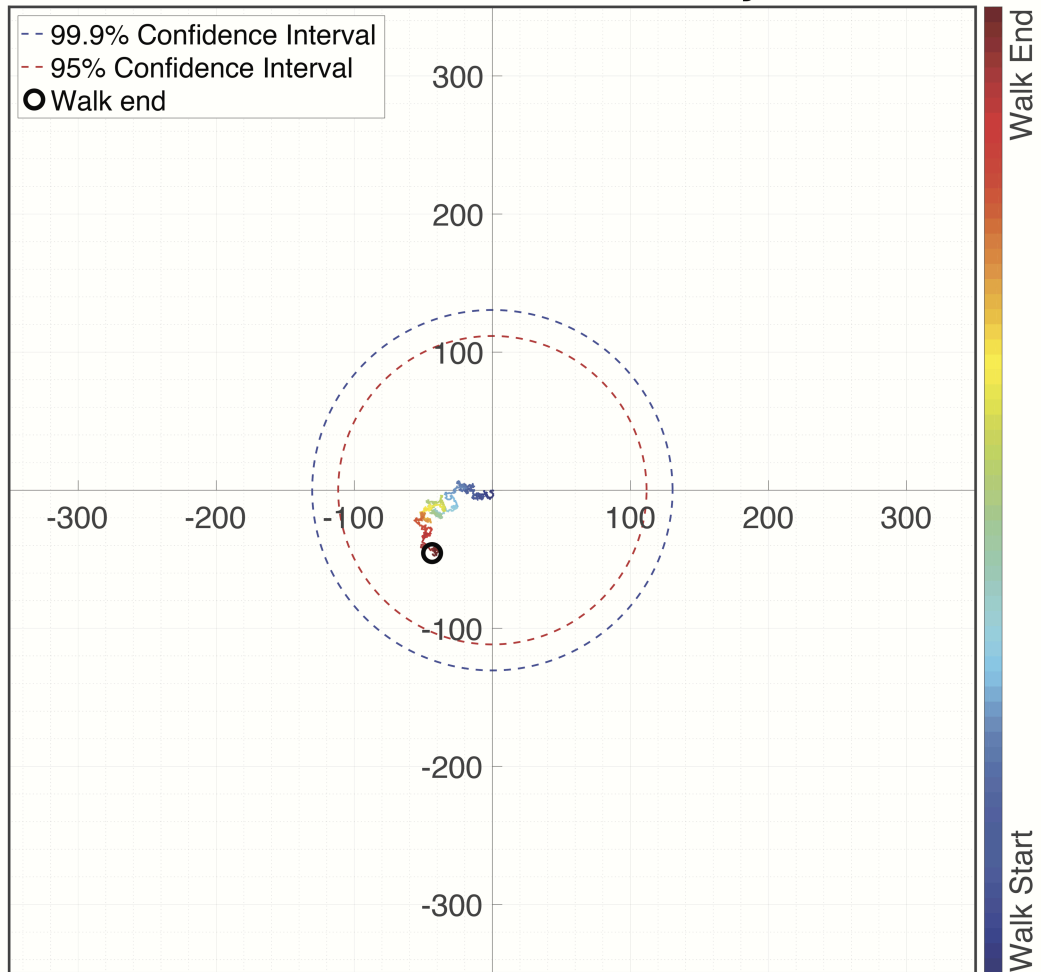


Figure 6. Schuster walk of declustered LFE family 9 tested at the tidal period of N2 (12.658 hr) with a result unable to reject the null hypothesis of uniform seismicity. Walk initiates at the origin in dark blue and finishes inside the black circle in dark red. The blue and red dashed lines represent the 99.9% and 95% confidence intervals respectively. The black outlined circle locates the walk's end. The test returns a significant result when the walk ends outside of the respective confidence interval. The test returns a significant result when the walk ends outside of the respective confidence interval.

## Percent Excess

The magnitudes of stresses in the crust induced by body tides are on the order of kPa. Previous work by Thomas et al. (2012) computed the tidally induced stress components consisting of the right-lateral shear stress (RLSS), fault-normal stress (FNS), and their time derivatives (dRLSS and dFNS). A 15-day time series of the FNS and RLSS is shown in Figure 7.

In order to evaluate the correlation of LFE events with tidal loading, we employed methodology from Thomas et al. (2009). Percent excess,  $N_{ex}$ , is the value of excess events calculated by the following equation

$$N_{ex} = \frac{(O-E)}{E}$$

where  $O$  is the observed frequency of events and  $E$  is the expected frequency of events. The expected number events,  $E$ , is the number of events that occur under a specified loading condition assuming that LFEs occurrence times are randomly distributed with respect to time. The loading conditions of interest include the signs of both the stress components and their derivatives. Four load components we analyze are tidally induced right-lateral shear stress (RLSS), right-lateral shear stress rate (dRLSS), fault normal stress (FNS), and fault normal stress rate (dFNS). The  $N_{ex}$  value represents a percentage surplus or deficit of events when positive or negative respectively. In this analysis we examine  $N_{ex}$  values of all individual LFE families by first calculating  $O$ , the total number

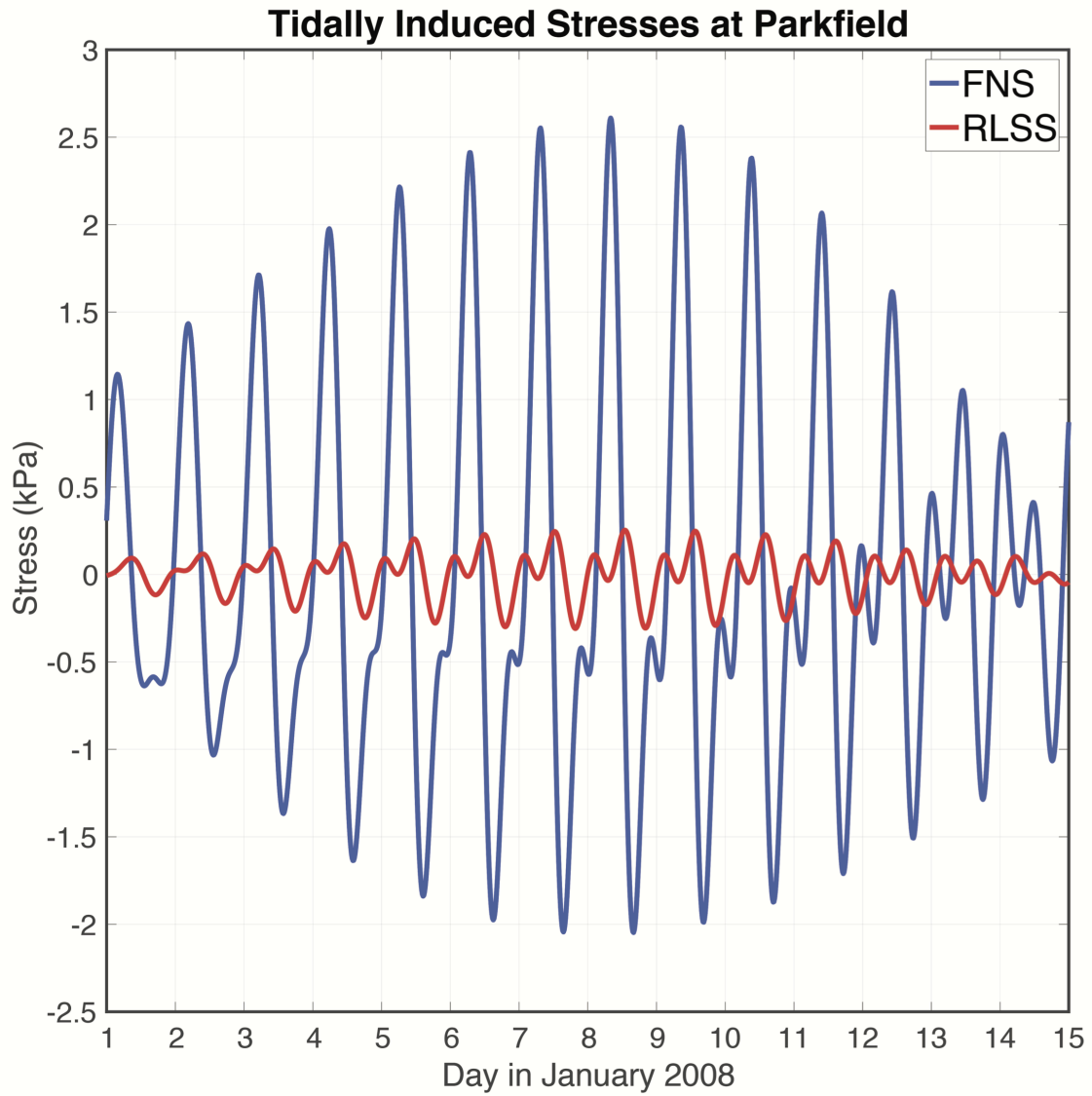


Figure 7. Time series of tidally induced shear (red) and normal (blue) stresses computed over a period of approximately two weeks for the SAF striking N42°W beneath Parkfield.

of events that occur during times of positive tidally induced stress. The percent of time a given family spends in a state of positive tidally induced stress is computed and then multiplied by the total number of events in that family's catalog, giving the value  $E$ . When used in the above equation, the resulting  $N_{ex}$  value can be used to evaluate to what degree an LFE family correlates with a given tidal component. To determine the confidence interval of a  $N_{ex}$  value for a given LFE family, a synthetic catalog is created by randomly distributing the total number events between the first and last event of the original catalog; this process is repeated to create 50,000 synthetic catalogs. The  $N_{ex}$  values are calculated for each synthetic catalog and the distribution of values is used to construct a two-sided 95% confidence interval. This is repeated across all LFE families for the RLSS, FNS, dRLSS, dFNS components.

## CHAPTER III

### RESULTS

#### **Schuster Spectra**

Schuster spectra of LFE families from the original catalog compared to the declustered families from the catalog of Thomas et al. (2018) indicate successful declustering of the catalog. Spurious p-values across many periods tested from the original catalog vanish, revealing significant p-values at the known tidal periods of highest amplitudes. To illustrate this, the Schuster spectrum of the original catalog of LFE family 9 (Fig. 8) shows hundreds of significant periods, each indicating a significant non-random component to seismicity at the respective periods. The Schuster spectrum of the declustered catalog of LFE family 9 (Fig. 9) indicates significant p-values at the known tidal periods of S2, M2, K1, and Q1, with all other periods resulting in values below the significance threshold.

Figure 10 shows the results of the Schuster spectra for all continuous (Fig. 10a) and episodic (Fig. 10b) LFE families. All continuous families to the north of Parkfield have at least one tidal period with a significant p-value, with most having more than two. All but four continuous families to the south of Parkfield have at least one tidal period with a significant p-value, with just over half having two or more. Episodic families with significant p-values only exist for four families with respect to period K1.

#### **Spatial Distribution of LFE Family Sensitivity to Tidal Stresses**

The sensitivity to tidal stresses for each LFE family was calculated and plotted for family locations along strike and with depth. Figure 11a shows the cross section of the

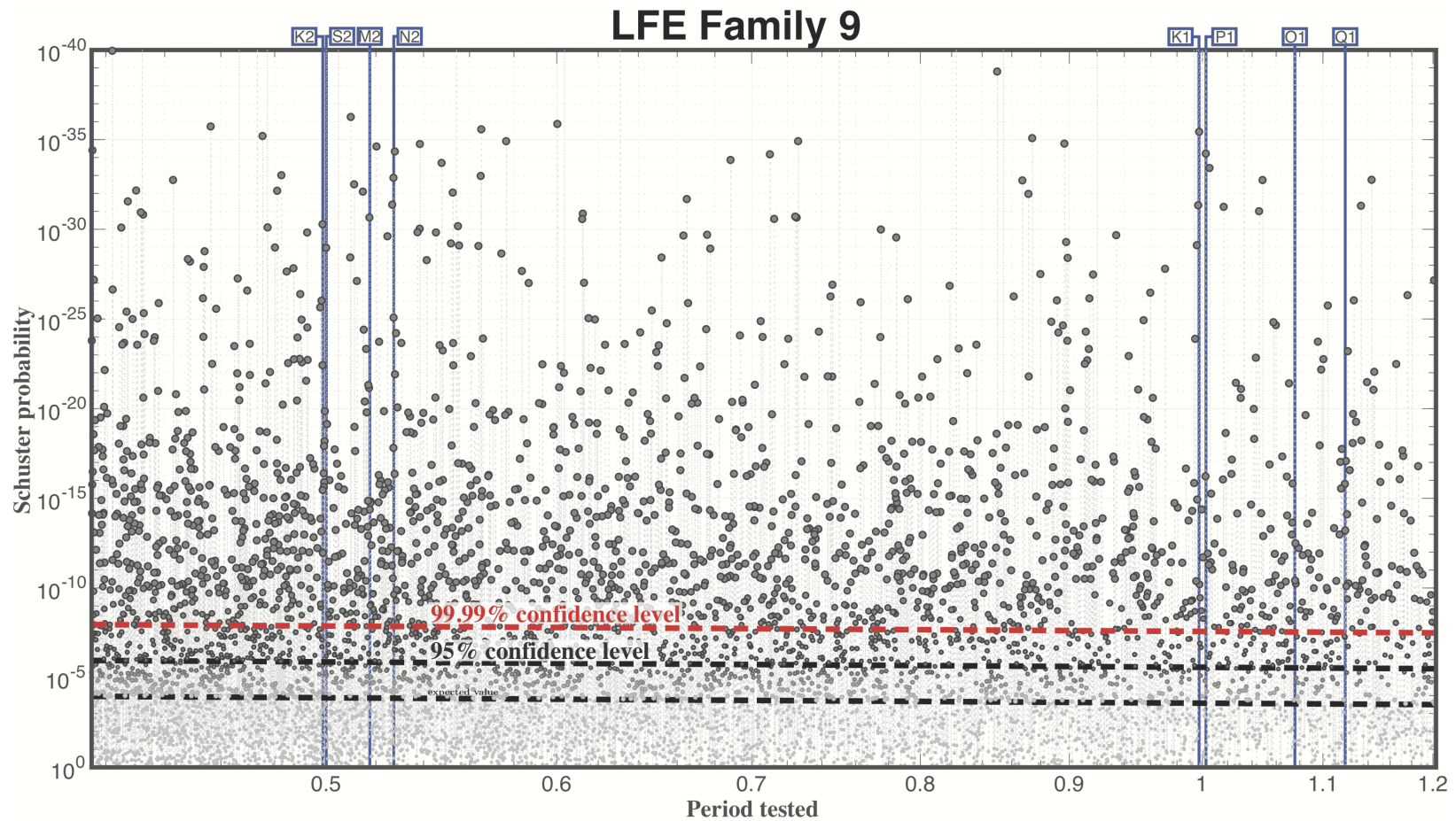


Figure 8. Schuster spectrum of original LFE family 9 catalog. The eight tidal periods that dominate in magnitude at Parkfield are shown as blue vertical lines, with the respective tidal symbols above in the attached blue boxes. The 99.99% confidence interval is shown in a dashed red line. Each grey circle represents the p-value calculated at the respective period tested, in units of days, on the x-axis. Many periods tested return significant p-values, indicating a high probability of a non-uniform component to seismicity at the respective period tested.

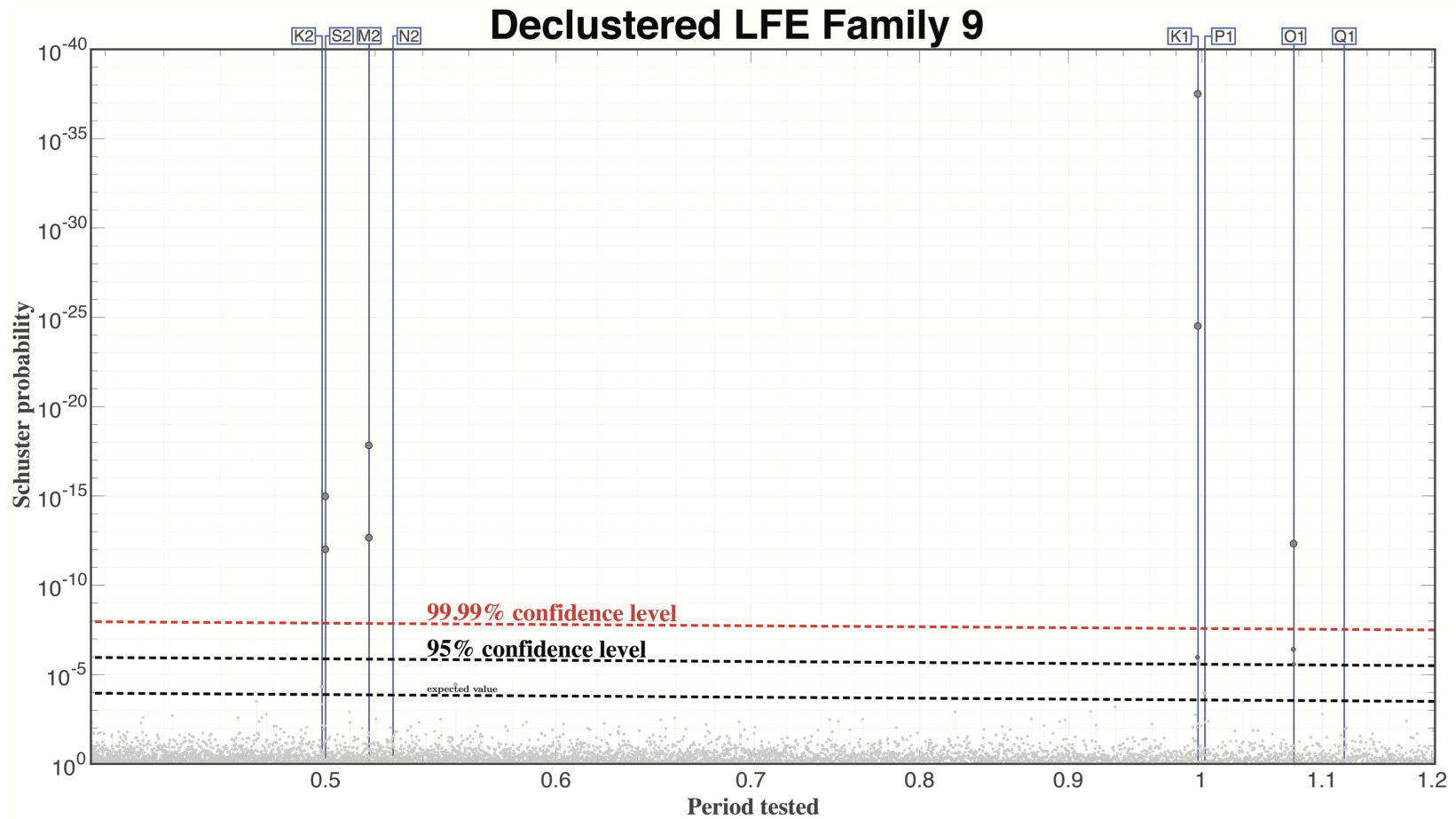


Figure 9. Schuster spectrum of declustered LFE family 9 catalog. The eight tidal periods that dominate in magnitude at Parkfield are shown as blue vertical lines, with the respective tidal symbols above in the attached blue boxes. The 99.99% confidence interval is shown in a dashed red line. Each grey circle represents the p-value calculated at the respective period tested, in units of days, on the x-axis. After declustering, spurious correlations disappear leaving only periods of the earth tides with significant p-values signifying non-uniform components to seismicity at the respective periods, indicating a successfully declustered catalog.





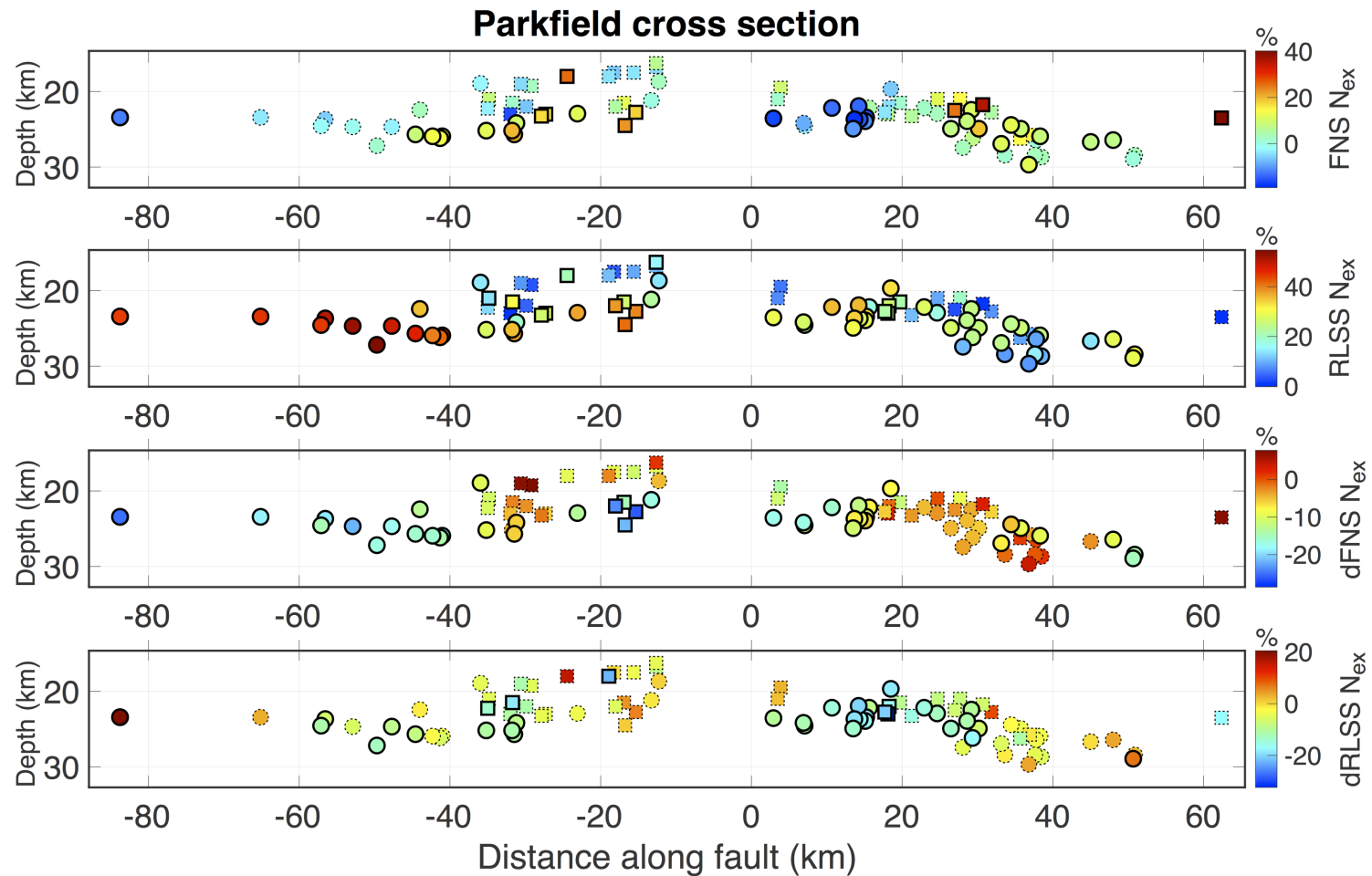


Figure 11. Cross section of SAF centered beneath Parkfield (0 km) with LFE locations color-coded by  $N_{ex}$  values and plotted as circles and squares, representing continuous and episodic families, respectively. From top to bottom, each panel represents the  $N_{ex}$  values calculated with respect to FNS, RLSS, dFNS, and dRLSS tidal components. Significant  $N_{ex}$  values are indicated via solid outlines and values falling below the confidence level of 95% are indicated via dashed lines.

SAF with the 88 LFE families identified by Shelly and Hardebeck (2010). For the subsequent panels, each family is color-coded by its sensitivity to the respective stressing condition ( $N_{ex}$  value). Overall, all 54 continuous families correlate with at least one tidal component tested. Of the 34 episodic families, 15 do not correlate with any tidal component tested. Figure 11b shows families' correlation with tensile (positive) FNS. A group of 8 continuous families between ~3-15 km (locked section southeast of Parkfield) shows a significant deficit in events. Below the creeping section of the SAF northwest of Parkfield, significant families correlate with tensile FNS with the exception of families 1 and 2. Of families correlating with tensile FNS, episodic families contain the highest  $N_{ex}$  values compared to continuous families. Figure 11c shows families' correlation with positive RLSS. All continuous families are correlated with RLSS at a significance level of 95% or greater. Sensitivity to shear stress varies systematically along strike, with the most sensitive families located to the northwest beneath the creeping section, decreasing in excess events towards families situated beneath the locked segment in the southeast. Of the significant episodic families with respect to the RLSS component, 10 out of 14 are located below the creeping section of the SAF. The four episodic families on the locked portion of the fault that do display significance are clustered in space. To the southeast of Parkfield, families decrease in their magnitudes of sensitivity from approximately 30% to just under 10% further to the southeast. Figure 11c shows families' correlation with dFNS. The significance of these values were found by Thomas et al. (2012) to be due to spurious correlation with RLSS. Figure 11d shows families' correlation with dRLSS. All but two significant families indicate a deficit with respect to dRLSS.

### **RLSS $N_{ex}$ vs Declustered RLSS $N_{ex}$**

Figure 12 shows  $N_{ex}$  values for the original catalogs of LFE families plotted against  $N_{ex}$  values of declustered LFE families for the RLSS tidal component. All 56 continuous LFE families retain a positive correlation indicating significantly more events than expected during times of positive RLSS. For episodic families, 14 of 32 have significantly more events than expected. Continuous families on the creeping section of the SAF are increasingly sensitive to RLSS from southeast to northwest. Episodic families tend to have less of a surplus of events compared to the original catalog. The gap in values between 18-21% from original catalogs is not as clearly preserved in declustered catalogs. The declustered values of episodic families are more scattered compared to declustered continuous families.

# RLSS $N_{ex}$

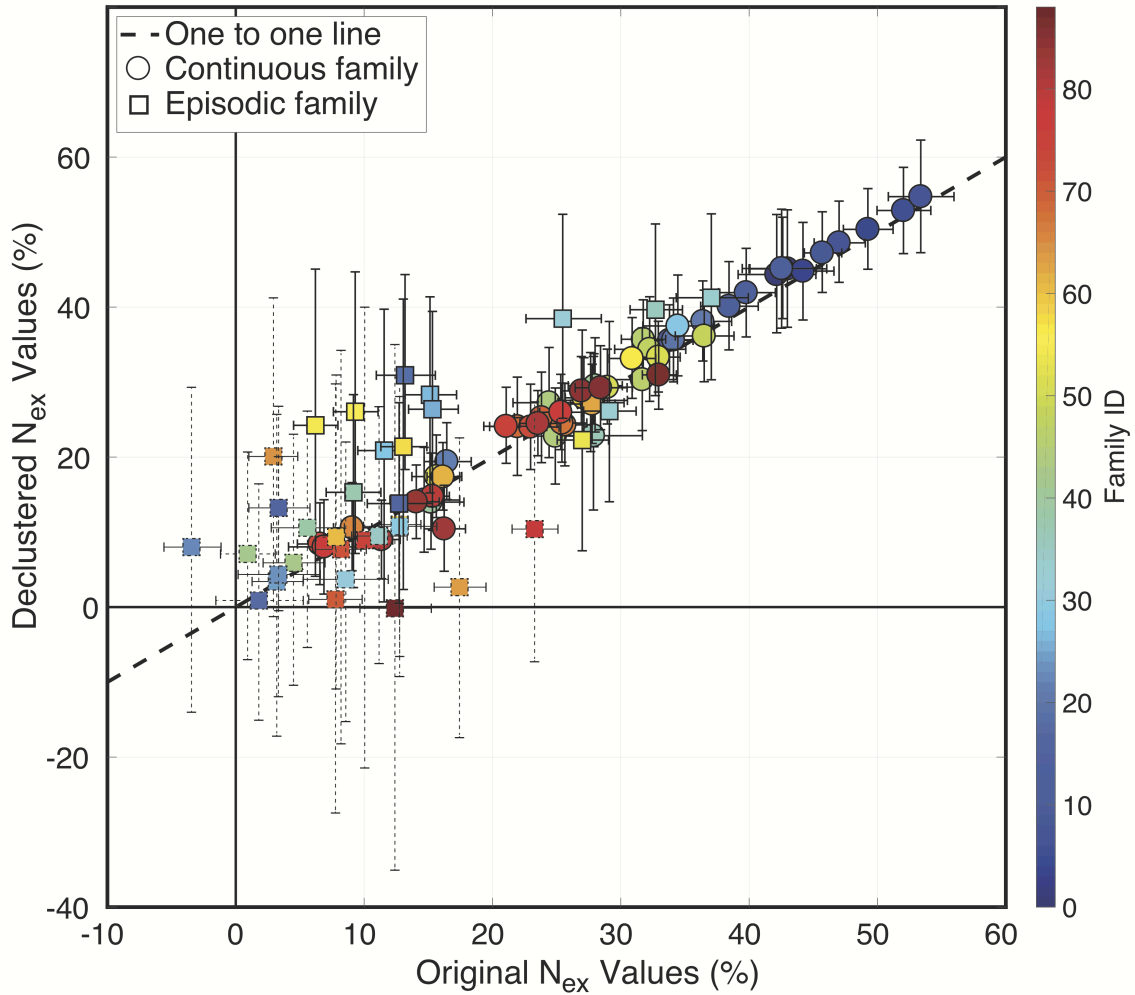


Figure 12. Original LFE catalog  $N_{ex}$  values plotted against declustered LFE catalog  $N_{ex}$  values plotted as circles and squares, representing continuous and episodic families, respectively. Solid error bars and symbol outlines indicate significant  $N_{ex}$  values, whereas dashed error bars and symbol outlines indicate insignificant  $N_{ex}$  values. Error bars represent the 95% confidence interval.

## CHAPTER IV

### DISCUSSION

The influence of tides on tremor and LFEs has been studied around the world, with significant tidal correlations discovered in subduction zones beneath Japan (Shelly et al., 2007a; Nakata et al., 2008; Ide, 2012; Ide and Tanaka, 2014; Yabe et al., 2015), Cascadia (Rubinstein et al., 2008; Lambert et al., 2009; Royer et al., 2014), and Taiwan (Chen et al., 2018). In an effort to further this field of study, the robust nature of LFEs sensitivity to tidal influences on the San Andreas Fault centered beneath Parkfield is discussed hereafter.

Previous work on this research area was conducted by Thomas et al. (2012), who established tidal sensitivity of LFE families on the SAF. An underlying assumption for the Schuster test and Schuster spectra is the independence of events from one another. The naturally clustered nature of LFE events violates this assumption and could potentially bias results. In an effort to further validate the previous work's results, we conducted analyses using a declustered version of the LFE catalog from Thomas et al. (2018).

#### **$N_{ex}$ Values**

Analysis of the declustered catalogs returned significant  $N_{ex}$  values with respect to the right-lateral shear stress tidal component for all 54 continuous LFE families and 15 of 34 episodic families. These results substantiate previous work analyzing tidal influence on the LFE families of the original LFE catalogs, confirming a widespread influence of RLSS on continuous LFE families (Thomas et al. 2012). Families that correlate with tensile (positive) FNS on the creeping section locate more deeply than the neighboring

insignificant families. These families were identified by Thomas et al. as correlating highly with FNS and they have retained their significance after declustering (2012). Another noteworthy collection of families is the cluster correlating negatively with tensile FNS along the stretch of the fault from 3-15 km southeast of Parkfield. This group has retained its significance from previous investigation and was found to exist on a releasing right bend of the SAF, which experiences fault-normal clamping (Thomas et al. 2012).

When calculating  $N_{ex}$  values, as the population of events in a family's catalog decreases, the confidence intervals increase. Declustering of episodic families results in a large reduction of events. A single burst of events in an episodic family can contain hundreds of events (Fig. 2 Family 55, Fig. 4), of which only the initiating event is kept. In addition, the average recurrence interval can be longer than 30 days. This drastic reduction in total events for an episodic family can remove more than 90% of its original catalog. Because the catalog still spans approximately the same length in time with many fewer events, the variation of random event distribution results in the increased span of confidence intervals. This effect could explain the reduction of total significant episodic LFE families with respect to given tidal components compared to previous work by Thomas et al. (2012). Another potential influence on the change in episodic families could be caused by the clustered character of their seismicity. After prolonged periods of quiescence, episodic families experience large bursts of events during periods of accelerated background slip. Thomas et al. suggest the magnitude of the background fault slip is much larger than the weaker tidal stress contribution during an active slip episode, resulting in the lack of significant tidal influence in episodic families (2012).

## Schuster Spectra

The Schuster spectrum was computed for original and declustered catalogs for all LFE families. The purpose of this analysis was twofold. Schuster spectra are suitable for determining whether a seismic catalog has been properly declustered, as well as detecting unknown periodicities within the catalog (Ader and Avouac, 2013). Figures 8 and 9 illustrate both of these results. Prior to declustering, LFE families typically experience seismicity in bursts, ranging from just a few events for continuous families to hundreds of events in episodic families. The clustered nature of this seismicity results in extremely low p-values across many periods tested in the Schuster spectra (Fig. 8), each of which corresponds to the probability that seismicity at the respective period resulted from uniform random process. Successful declustering of the catalog removes these spurious correlations, which allows for genuine periodic perturbations to be resolved (Figure 9).

The aggregate results of the Schuster spectra for the declustered catalogs are shown in Figure 10. Continuous LFE families that correlate with tidal constituents far outnumber episodic families and also show a difference in sensitivity between the creeping (Families 1-40) and locked (Families 41-88) segments of the fault. The deeper continuous families beneath the creeping section, which have the highest  $N_{ex}$  values for the RLSS component, are also influenced by multiple tidal constituents. Beneath the locked segment continuous families are less influenced overall, especially by tidal constituents O1 and S2. The tidal components ranked in order of highest to lowest amplitudes calculated from the tidal stress time series are K1, M2, O1, S2, P1, N2, Q1, and K2 (Table 1). For RLSS, the tidal constituents ranked from highest to lowest are M2, S2, K1, O1, P1, K2, N2, and Q1 (Table 1). In decreasing order, the total number of

families with significant values from the Schuster test at the respective period are K1, M2, S2, and O1. Generally, the larger tidal constituents correlate more strongly than weaker constituents. Constituents with amplitudes smaller than S2 are not present on the Schuster spectra except for the case of K1/P1. P1 ranks as the fifth largest tidal constituent for Parkfield, CA. Exactly halfway between K1 and P1 is a tidal period of S1, with a period of 24 hours. This constituent does not contribute an appreciable amplitude for the area of Parkfield, or even globally (Ray and Egbert, 2004). Because the phases of K1 and P1 vary by less than three degrees when using the Schuster test, it is possible that the families with significant p-values between the periods K1 and P1 result from the superposition of their individual amplitudes. Only four episodic LFE families (32, 33, 34, 36) return significant values at the largest period, K1. These four families cluster closely between 15-18 km north of Parkfield with depths ~21-23 km and had the highest significant  $N_{ex}$  values of episodic families with respect to the RLSS tidal component.

These results indicate that stresses induced by solid earth tides modulate seismicity of individual LFE families. Continuous families, which are generally located deeper on the fault, experience deformation more often than do episodic families, as shown by the more frequent and small bursts of activity for continuous families. Their activity is more readily influenced by small induced RLSS, with  $N_{ex}$  values of almost 50% for some families, as well as their cyclic modulations by tidal constituents across the fault. Episodic families overall respond less strongly to induced RLSS, and they lack significant modulation on the scale of individual tidal constituents.

The significant correlation of LFEs with tidally induced RLSS has been used to infer fault rheology in the LFE source region. To generate seismic slip on an asperity at



depths between 15-30 km, several conditions must be met. Tremor must manifest from shear failure producing seismic radiation (Ide et al., 2007), which requires brittle failure of the LFE source. Beeler et al. (2013) concluded that ductile mineral flow mechanisms of dislocation glide and creep are inconsistent with observed fault creep, advocating for brittle-frictional behavior as the method for explaining tide-LFE correlation. The LFE source fails seismically as it is loaded by stress from both aseismic creep of the larger-scale surrounded fault zone (Shelly et al., 2007) in addition to the solid earth tides (Beeler et al., 2013). Deep brittle failure sensitive to small stress perturbations can only occur if the fault has low effective normal stress (Thomas et al. 2009, 2012; Beeler et al., 2013, 2018). Low effective normal stress is achieved through high pore fluid pressure on the order of lithostatic pressure (Thomas et al., 2009), which has been imaged by geophysical surveys of the region (Becken et al., 2011). The lack of LFE correlation to FNS can also be explained by pore fluid pressure. Hawthorne et al. (2010) found changes in normal stress cause changes in pore pressure, which dampens the magnitude of FNS on the fault by more than 90%, assuming hydraulic diffusivity is sufficiently low on the tidal time scale.

## CHAPTER IV

### CONCLUSIONS

This study analyzed the tidal sensitivity of declustered LFE families on the SAF centered at Parkfield, CA. The goal was to validate previous work by Thomas et al. (2012) using a declustered LFE catalog to satisfy the statistical analyses' underlying assumptions of independent events. We first used the Schuster test and its extension, the Schuster spectrum, to evaluate the declustering of the LFE catalog from Thomas et al. (2018). In addition, the Schuster spectra allowed for the detection of periods containing a significant nonrandom component to seismicity in LFE families, providing a more detailed view of tidal influence on LFE families along the SAF. Percent excess calculations were performed for each family using the declustered catalog as well.

Schuster spectra from the original catalog were compared to those from the declustered catalog of Thomas et al. and indicated a successful declustering, demonstrated by the extensive reduction in spurious significant results across the timescales of interest. Percent excess results confirmed the extreme sensitivity of LFEs to tidally induced stresses, with all continuous LFE families resulting in significant excess events during times of positive RLSS. Continuous LFE families on the northern creeping segment of SAF have higher  $N_{ex}$  values compared to those located on the southern locked segment, suggesting the creeping section is more amenable to deformation and small stress changes. The cluster of LFE families was negatively correlated with tensile FNS along the fault 3-15 km southeast of Parkfield after declustering.

Episodic families exhibit a decrease in overall sensitivity to tidal stress likely due to the combination of decreased catalog events and larger background fault slip during

active episodes. Schuster spectra results suggest a general trend of increased tidal stress amplitudes at given periods influencing more LFE families, as well as the spatial heterogeneity of LFE sensitivity between the creeping and locked regions of the SAF. This study therefore corroborates the correlation of LFEs with solid earth tides and upholds the inference that low effective stress facilitates frictional slip on the deep SAF (Thomas et al. 2009; 2012; Beeler et al. 2013; 2018).

## REFERENCES CITED

- Ader, T. J., & Avouac, J. P. (2013). Detecting periodicities and declustering in earthquake catalogs using the Schuster spectrum, application to Himalayan seismicity. *Earth and Planetary Science Letters*, 377, 97-105.
- Agnew, D. C. (2005). Earth tides: an introduction. *Univer. California, San Diego, CA, USA*.
- Argus, D. F., & Gordon, R. G. (2001). Present tectonic motion across the Coast Ranges and San Andreas fault system in central California. *Geological Society of America Bulletin*, 113(12), 1580-1592.
- Baker, T. F. (1984). Tidal deformations of the Earth. *Science Progress Oxford*, 69, 197-233.
- Becken, M., Ritter, O., Bedrosian, P. A., & Weckmann, U. (2011). Correlation between deep fluids, tremor and creep along the central San Andreas fault. *Nature*, 480(7375), 87.
- Beeler, N. M., Thomas, A., Bürgmann, R., & Shelly, D. (2013). Inferring fault rheology from low-frequency earthquakes on the San Andreas. *Journal of Geophysical Research: Solid Earth*, 118(11), 5976-5990.
- Beeler, N. M., Thomas, A., Bürgmann, R., & Shelly, D. (2018). Constraints on Friction, Dilatancy, Diffusivity, and Effective Stress From Low-Frequency Earthquake Rates on the Deep San Andreas Fault. *Journal of Geophysical Research: Solid Earth*, 123(1), 583-605.
- Beroza, G. C., & Ide, S. (2011). Slow earthquakes and nonvolcanic tremor. *Annual review of Earth and planetary sciences*, 39, 271-296.
- Burford, R. O., & Harsh, P. W. (1980). Slip on the San Andreas fault in central California from alignment array surveys. *Bulletin of the Seismological Society of America*, 70(4), 1233-1261.
- Chen, K. H., Tai, H. J., Ide, S., Byrne, T. B., & Johnson, C. W. (2018). Tidal modulation and tectonic implications of tremors in Taiwan. *Journal of Geophysical Research: Solid Earth*, 123(7), 5945-5964.
- Dragert, H., Wang, K., & James, T. S. (2001). A silent slip event on the deeper Cascadia subduction interface. *Science*, 292(5521), 1525-1528.
- Dragert, H., Wang, K., & Rogers, G. (2004). Geodetic and seismic signatures of episodic tremor and slip in the northern Cascadia subduction zone. *Earth, planets and space*, 56(12), 1143-1150.

- Frey Mueller, J. T., Hreinsdóttir, S., Zweck, C., & Haeussler, P. J. (2002, December). The 1998-2002 deep megathrust slip event, Alaska. In *AGU Fall Meeting Abstracts*.
- Gomberg, J., Rubinstein, J. L., Peng, Z., Creager, K. C., Vidale, J. E., & Bodin, P. (2008). Widespread triggering of nonvolcanic tremor in California. *Science*, *319*(5860), 173-173.
- Hirose, H., & Obara, K. (2005). Repeating short-and long-term slow slip events with deep tremor activity around the Bungo channel region, southwest Japan. *Earth, planets and space*, *57*(10), 961-972.
- Hirose, H., Hirahara, K., Kimata, F., Fujii, N., & Miyazaki, S. I. (1999). A slow thrust slip event following the two 1996 Hyuganada earthquakes beneath the Bungo Channel, southwest Japan. *Geophysical Research Letters*, *26*(21), 3237-3240.
- Ide, S. (2012). Variety and spatial heterogeneity of tectonic tremor worldwide. *Journal of Geophysical Research: Solid Earth*, *117*(B3).
- Ide, S., & Tanaka, Y. (2014). Controls on plate motion by oscillating tidal stress: Evidence from deep tremors in western Japan. *Geophysical Research Letters*, *41*(11), 3842-3850.
- Ide, S., Beroza, G. C., Shelly, D. R., & Uchide, T. (2007a). A scaling law for slow earthquakes. *Nature*, *447*(7140), 76.
- Ide, S., Shelly, D. R., & Beroza, G. C. (2007b). Mechanism of deep low frequency earthquakes: Further evidence that deep non-volcanic tremor is generated by shear slip on the plate interface. *Geophysical Research Letters*, *34*(3).
- Ito, Y., Obara, K., Shiomi, K., Sekine, S., & Hirose, H. (2007). Slow earthquakes coincident with episodic tremors and slow slip events. *Science*, *315*(5811), 503-506.
- Kao, H., Shan, S. J., Dragert, H., Rogers, G., Cassidy, J. F., & Ramachandran, K. (2005). A wide depth distribution of seismic tremors along the northern Cascadia margin. *Nature*, *436*(7052), 841.
- Lambert, A., Kao, H., Rogers, G., & Courtier, N. (2009). Correlation of tremor activity with tidal stress in the northern Cascadia subduction zone. *Journal of Geophysical Research: Solid Earth*, *114*(B8).
- Lowry, A. R., Larson, K. M., Kostoglodov, V., & Bilham, R. (2001). Transient fault slip in Guerrero, southern Mexico. *Geophysical Research Letters*, *28*(19), 3753-3756.

- Miyazawa, M., & Brodsky, E. E. (2008). Deep low-frequency tremor that correlates with passing surface waves. *Journal of Geophysical Research: Solid Earth*, 113(B1).
- Murray, M. H., & Segall, P. (2001). Modeling broadscale deformation in northern California and Nevada from plate motions and elastic strain accumulation. *Geophysical Research Letters*, 28(22), 4315-4318.
- Nadeau, R. M., & Dolenc, D. (2005). Nonvolcanic tremors deep beneath the San Andreas Fault. *Science*, 307(5708), 389-389.
- Nadeau, R. M., & Guilhem, A. (2009). Nonvolcanic tremor evolution and the San Simeon and Parkfield, California, earthquakes. *science*, 325(5937), 191-193.
- Nakata, R., Suda, N., & Tsuruoka, H. (2008). Non-volcanic tremor resulting from the combined effect of Earth tides and slow slip events. *Nature Geoscience*, 1(10), 676.
- Nishide, N., Hashimoto, T., Funasaki, J., Nakazawa, H., Oka, M., Ueno, H., ... & Takashima, T. (2000). Nationwide activity of low-frequency earthquakes in the lower crust in Japan. In *Abstr. Jpn. Earth and Planet. Sci. Joint Meeting*, sk-p002.
- Obara, K. (2002). Nonvolcanic deep tremor associated with subduction in southwest Japan. *Science*, 296(5573), 1679-1681.
- Obara, K., & Hirose, H. (2006). Non-volcanic deep low-frequency tremors accompanying slow slips in the southwest Japan subduction zone. *Tectonophysics*, 417(1-2), 33-51.
- Obara, K., Hirose, H., Yamamizu, F., & Kasahara, K. (2004). Episodic slow slip events accompanied by non-volcanic tremors in southwest Japan subduction zone. *Geophysical Research Letters*, 31(23).
- Ozawa, S., Murakami, M., & Tada, T. (2001). Time-dependent inversion study of the slow thrust event in the Nankai trough subduction zone, southwestern Japan. *Journal of Geophysical Research: Solid Earth*, 106(B1), 787-802.
- Peng, Z., Vidale, J. E., Wech, A. G., Nadeau, R. M., & Creager, K. C. (2009). Remote triggering of tremor along the San Andreas Fault in central California. *Journal of Geophysical Research: Solid Earth*, 114(B7).
- Ray, R. D., & Egbert, G. D. (2004). The global S1 tide. *Journal of Physical Oceanography*, 34(8), 1922-1935.
- Rogers, G., & Dragert, H. (2003). Episodic tremor and slip on the Cascadia subduction zone: The chatter of silent slip. *Science*, 300(5627), 1942-1943.

- Rogers, G., & Dragert, H. (2003). Episodic tremor and slip on the Cascadia subduction zone: The chatter of silent slip. *Science*, *300*(5627), 1942-1943.
- Royer, A. A., Thomas, A. M., & Bostock, M. G. (2015). Tidal modulation and triggering of low-frequency earthquakes in northern Cascadia. *Journal of Geophysical Research: Solid Earth*, *120*(1), 384-405.
- Rubinstein, J. L., La Rocca, M., Vidale, J. E., Creager, K. C., & Wech, A. G. (2008). Tidal modulation of nonvolcanic tremor. *Science*, *319*(5860), 186-189.
- Rubinstein, J. L., Vidale, J. E., Gomberg, J., Bodin, P., Creager, K. C., & Malone, S. D. (2007). Non-volcanic tremor driven by large transient shear stresses. *Nature*, *448*(7153), 579.
- Ryder, I., & Bürgmann, R. (2008). Spatial variations in slip deficit on the central San Andreas fault from InSAR. *Geophysical Journal International*, *175*(3), 837-852.
- Schmidt, D. A., & Gao, H. (2010). Source parameters and time-dependent slip distributions of slow slip events on the Cascadia subduction zone from 1998 to 2008. *Journal of Geophysical Research: Solid Earth*, *115*(B4).
- Scholz, C. H. (2002). *The mechanics of earthquakes and faulting*. Cambridge university press.
- Schulz, S. S., Mavko, G. M., Burford, R. O., & Stuart, W. D. (1982). Long-term fault creep observations in central California. *Journal of Geophysical Research: Solid Earth*, *87*(B8), 6977-6982.
- Schuster, A. (1897). On lunar and solar periodicities of earthquakes. *Proceedings of the Royal Society of London*, *61*(369-377), 455-465.
- Schwartz, S. Y., & Rokosky, J. M. (2007). Slow slip events and seismic tremor at circum-Pacific subduction zones. *Reviews of Geophysics*, *45*(3).
- Shelly, D. R., & Hardebeck, J. L. (2010). Precise tremor source locations and amplitude variations along the lower-crustal central San Andreas Fault. *Geophysical Research Letters*, *37*(14).
- Shelly, D. R., & Johnson, K. M. (2011). Tremor reveals stress shadowing, deep postseismic creep, and depth-dependent slip recurrence on the lower-crustal San Andreas fault near Parkfield. *Geophysical Research Letters*, *38*(13).
- Shelly, D. R., Beroza, G. C., & Ide, S. (2007a). Complex evolution of transient slip derived from precise tremor locations in western Shikoku, Japan. *Geochemistry, Geophysics, Geosystems*, *8*(10).

- Shelly, D. R., Beroza, G. C., & Ide, S. (2007b). Non-volcanic tremor and low-frequency earthquake swarms. *Nature*, 446(7133), 305.
- Shelly, D. R., Beroza, G. C., Ide, S., & Nakamura, S. (2006). Low-frequency earthquakes in Shikoku, Japan, and their relationship to episodic tremor and slip. *Nature*, 442(7099), 188.
- Sieh, K. E. (1978). Slip along the San Andreas fault associated with the great 1857 earthquake. *Bulletin of the Seismological Society of America*, 68(5), 1421-1448.
- Thatcher, W., & Lisowski, M. (1987). Long-term seismic potential of the San Andreas fault southeast of San Francisco, California. *Journal of Geophysical Research: Solid Earth*, 92(B6), 4771-4784.
- Thomas, A. M., Beeler, N. M., Bletery, Q., Burgmann, R., & Shelly, D. R. (2018). Using Low-Frequency Earthquake Families on the San Andreas Fault as Deep Creepmeters. *Journal of Geophysical Research: Solid Earth*, 123(1), 457-475.
- Thomas, A. M., Bürgmann, R., Shelly, D. R., Beeler, N. M., & Rudolph, M. L. (2012). Tidal triggering of low frequency earthquakes near Parkfield, California: Implications for fault mechanics within the brittle-ductile transition. *Journal of Geophysical Research: Solid Earth*, 117(B5).
- Thomas, A. M., Nadeau, R. M., & Bürgmann, R. (2009). Tremor-tide correlations and near-lithostatic pore pressure on the deep San Andreas fault. *Nature*, 462(7276), 1048.
- Waldhauser, F., & Schaff, D. P. (2008). Large-scale relocation of two decades of northern California seismicity using cross-correlation and double-difference methods. *Journal of Geophysical Research: Solid Earth*, 113(B8).
- Yabe, S., Tanaka, Y., Houston, H., & Ide, S. (2015). Tidal sensitivity of tectonic tremors in Nankai and Cascadia subduction zones. *Journal of Geophysical Research: Solid Earth*, 120(11), 7587-7605.